CHEMPHYSCHEM

DOI: 10.1002/cphc.200700793

Electrochemical Fabrication of Nanostructured Surfaces for Enhanced Response

Tesfaye Refera Soreta,[a] Jörg Strutwolf,*[a] and Ciara K. O'Sullivan*[a, b]

The objective of this work is to explore approaches to enhance electrochemical signals through sequential deposition and capping of gold particles. Gold nanoparticles are electrodeposited from $KAuCl_4$ solution under potentiostatic conditions on glassy carbon substrates. The number density of the nanoparticles is increased by multiple deposition steps. To prevent secondary nucleation processes, the nanoparticles are isolated after each potentiostatic deposition step by self-assembled monolayers (SAMs) of decanethiol or mercaptoethanol. The increasing number of particles during five deposition/protection rounds is monitored by assembling electroactive SAMs using a ferrocene-labeled alkanethiol. A precise estimation of the surface area of the gold nanoparticles by formation of an oxide layer on gold is difficult due to oxidation of the glassy carbon surface. As an alternative approach, the charge flow of the electroactive SAM is used for surface measurement of the gold surface area. A sixfold increase in the redox signal in comparison to a bulk gold surface is observed, and this increase in redox signal is particularly notable given that the surface area of the deposited nanoparticles is only a fraction of the bulk gold surface. After five rounds of deposition there is a gold loading of 1.94 $\mu g\,cm^{-2}$ of the deposited nanoparticles as compared to 23.68 $\mu g\,cm^{-2}$ for the bulk gold surface. Remarkably, however, the surface coverage of the ferrocene alkanethiol on the bulk material is only 10% of that achieved on the deposited nanoparticles. This enhancement in signal of the nanoparticle-modified surface in comparison to bulk gold is thus demonstrated not to be attributable to an increase in surface area, but rather to the inherent properties of the surface atoms of the nanoparticles, which are more reactive than the surface atoms of the bulk material.

Introduction

A major influence on electrode development over the last decade has been the progress in nanotechnology. The application of metal nanoparticles in electroanalytical and bioanalytical science has been a subject of continuously growing interest, as documented in recent reviews.[1–6] Nanoparticles have also had an important impact on electrocatalysis research,[1,7–11] for example, gold nanoparticles show excellent catalytic properties towards the electrochemical reduction of molecular oxygen[12–14] and towards the low-temperature oxidation of CO.[11,15] The electrocatalytic effect of gold nanoparticles on ascorbic acid oxidation allows the selective electrochemical analysis of dopamine and ascorbic acid[16,17] coexisting in biological liquids, whereas using conventional (bulk) Au electrodes, the oxidation waves of ascorbic acid have almost the same potential, which results in poor selectivity and reproducibility. The use of gold nanoparticles as labels has also been reported for electrochemical genosensors.[18,19] The technological prospects of the application of gold nanoparticle-based materials are a major motivation for the development and fabrication of nanoparticles with predetermined dimensions. Thus, substantial effort has been devoted to the preparation of size- and shape-controlled nanoparticles, particularly of metal nanoparticles for electroanalytical applications.[6,20]

One of the main reasons that nanomaterials show properties different from those of the bulk material is the size effect: atoms at the surface have lower coordination numbers and are therefore less stable than bulk atoms. The smaller a particle, the larger the fraction of atoms at the surface, and thus the more reactive is the surface, which makes nanosized materials of immense interest as substrates for biosensor applications.

Electrochemical deposition is a rapid and easy procedure for the production of nanoparticles on conducting surfaces, and many reports have been devoted to the electrodeposition of Au onto glassy carbon (GC).[17,21–26] The composite surface of GC modified with gold nanoparticles offers the possibility of further site-selective modification, as GC has no affinity towards thiol or disulfide groups in contrast to gold, on which thiol-based self-assembled monolayers (SAMs) are readily formed. Thus, it is possible to protect or selectively functionalize spots on an overall conducting surface. Finot et al.[24] used a SAM of octadecanethiol (ODT) to protect deposited Au nanocrystallites after the deposition step on GC electrodes. New gold nanoparticles were then electrodeposited from an aqueous $KAuCl_4$ solution without causing crystal growth of the par-

[a] *T. Refera Soreta, Dr. J. Strutwolf,[+] Dr. C. K. O'Sullivan*
Nanobiotechnology & Bioanalysis Group
Departament d'Enginyeria Quimica
Universitat Rovira i Virgili, 43007 Tarragona (Spain)
Fax: (+34) 977 559621
E-mail: ciara.osullivan@urv.cat

[b] *Dr. C. K. O'Sullivan*
Institució Catalana de Recerca i Estudis Avançats
Passeig Lluis Campanys 23, 08010 Barcelona (Spain)

[+] *Current address: Tyndall National Institute*
Lee Maltings, Cork (Ireland)
Fax: (+353) 21427-0271
E-mail: jorg.strutwolf@tyndall.ie

ticles deposited in the previous steps, which were protected by an ODT film. The deposition–protection sequence was repeated and, to prove that during each deposition step new Au crystallites were formed, the authors used the electron transfer (ET) of catechol at the GC surface, which is relatively slow in comparison to the ET rate at a gold substrate. After each Au deposition step, the peak potential separation of the cyclic voltammogram had the typical value of a reversible ET, while after blocking the Au crystallites with ODT, an increase of the peak separation indicated the nonreversible ET taking place at the GC surface.[24] The electrodeposition/SAM formation process was also used by El-Deab et al. to produce ternary SAMs on gold nanoparticles deposited on GC by domain-selective chemisorption/desorption of thiol compounds at three different domains of the Au crystallites.[27]

Herein, we report the exploitation of a multiple gold deposition/SAM formation sequence similar to the procedure used by Finot et al.,[24] but improving on the method by employing coadsorption of ferrocene-terminated and unsubstituted thiols on the gold nanoparticles to create electroactive SAMs[28,29] during each deposition/SAM formation step. This enables monitoring of the Au particle formation after each deposition/formation sequence by measuring the redox current of the attached ferrocene entity.

An extraordinary increase in the redox signal of the electroactive SAM of ferrocene-$C_{11}SH$ ($FcC_{11}SH$) is observed which cannot be attributed solely to the increase of gold surface area during each deposition step. A higher number of chemisorbed electroactive molecules per area is observed for nanoparticle-modified electrodes than for bulk gold, which is attributed to the inherent properties of the deposited nanoparticles.

Results and Discussion

The main interest of this work is to demonstrate a new scheme of nanostructured electrode preparation by the sequential deposition of gold nanoparticles as a strategy for signal amplification of redox-active labels for application in biosensors. Control over the size and distribution of electrodeposited gold nanoparticles is also demonstrated by combining previously reported approaches with the scheme reported here, and an electroactive labeled thiol was used to distinguish the GC electroactive surfaces from the gold nanoparticle deposits.

The sequential deposition/protection procedure is illustrated in Scheme 1. After electrochemical deposition, the gold nanoparticles on the GC surface are protected by the self-assembly of a thiol monolayer to prevent them from being used as seeds in the subsequent gold deposition step. In the next deposition step, new particles are mainly formed on the GC surface due to the insulating action of the SAM on the gold particles deposited in the previous step. By repeating this procedure, a higher density of isolated nanoparticles can be achieved with each cycle of deposition.

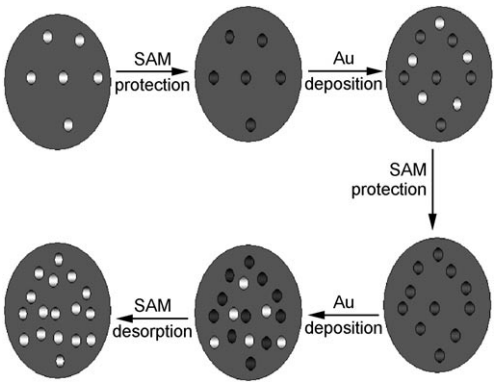

Scheme 1. The sequential electrodeposition/protection procedure for nanoparticle deposition on GC. White circles: unprotected particles; black circles: gold particles protected by a SAM. Three rounds of the deposition/protection sequence are shown.

Gold Nanoparticle Electrodeposition

A wide-potential cyclic voltammetric scan (Figure 1) of 1 mM $KAuCl_4$ in 0.5 M aqueous H_2SO_4 probes the most suitable potential for deposition of the gold particles. The voltammogram

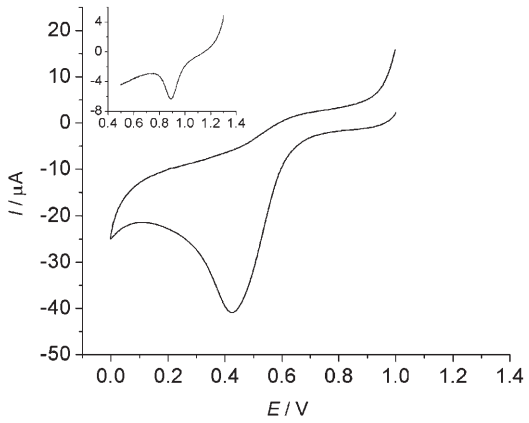

Figure 1. Cyclic voltammogram of 0.1 mM K_4AuCl_4 in 0.5 M H_2SO_4 using a GC electrode. Inset: reduction of a gold oxide layer formed on the deposited gold particles. Scan rate: 50 mV s^{-1}.

is very similar to that reported by Finot et al.,[23] with gold starting to deposit at a potential of +0.8 V with a peak potential at +0.51 V. The process is irreversible within the potential window studied. The presence of gold deposits is confirmed by the formation of a gold oxide layer followed by its reduction in the reverse scan, where the peak potential for reduction of gold oxide is +0.90 V (Figure 1, inset).

Gold nanoparticles are deposited from $KAuCl_4$ at concentrations of 1 mM and 0.1 mM. The deposition potential is varied between 0 and 600 mV and the deposition time of 1–25 s. Optimal conditions regarding particle size, distribution, and number density occur at an applied potential of 0 V for 5 s from a 0.1 mM $KAuCl_4$ solution, which is in agreement with the conditions reported by Finot et al.[23] The nanoparticles deposited using these parameters also show optimal characteristics

towards the formation of SAMs of ferrocene-labeled alkanethiols.

The nucleation mechanism of a metal is influenced by several factors,[34] such as the presence of organic additives,[35] the applied overpotential, and notably the nature of the substrate, as nucleation is proposed to initiate at the step edges and kink sites of the substrate. A rapid nucleation growth rate is observed, in agreement with Finot et al.,[23] due to the fast growth of the Au particles in the initial state. We were not able to experimentally access the rising portion of the transient under our conditions (transient time resolution 1 ms). However, an instantaneous nucleation process for gold on GC was reported.[36] In a progressive nucleation process particles are formed continuously during the application of the potential pulse, while instantaneous nucleation refers to a scenario where the timescale during which nucleation occurs is much shorter than the subsequent growth phase, which results in a more uniform particle-size dispersion. Therefore, to form uniform structures by metal deposition, instantaneous nucleation is desirable, in particular with the multiple-deposition experiments presented here.

Characterization of the Au Particles by SEM

Figure 2 presents typical scanning electron microscopy (SEM) images for the deposition of gold crystallites from 0.1 mM $KAuCl_4$ solution at a deposition potential of 0.0 V on GC. Figure 2A shows gold particles formed after a single 5 s potential step from 1.1 to 0 V. Figure 2B shows gold particles formed during three consecutive deposition steps (5 s each, step potential from 1.1 to 0 V), with a mercaptoethanol (ME) layer assembled on the particles after each deposition. Figure 2C is similar to Figure 2B, but decanethiol (DT) is used instead of ME for protecting the gold nanoparticles after each deposition step. For comparison, Figure 2D shows particles formed during three 5 s deposition steps without the use of a SAM as a protecting layer. The number of particles n for the single-step deposition (Figure 2A) is 187 μm^{-2}, measured over an area of 48 μm^2, while for the three deposition rounds with ME and DT SAMs (Figures 2B and C) n has values of 314 and 386 μm^{-2}, respectively. Three deposition rounds without SAM formation result in a particle density of 41 μm^{-2} (Figure 2D).

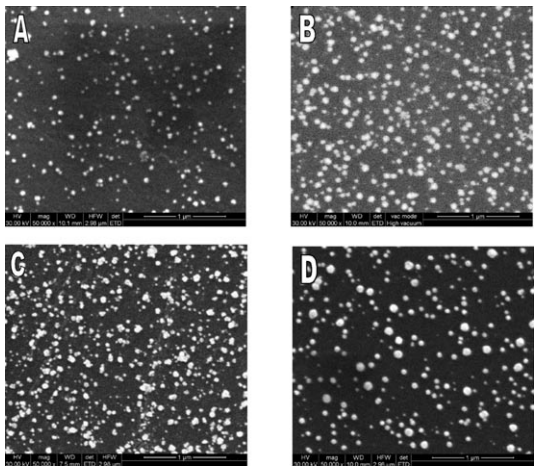

Figure 2. SEM images of electrochemically deposited gold nanoparticles on GC. Deposition potential: 0 V from 0.1 mM K_4AuCl_4 in 0.5 M aq. H_2SO_4. A) One 5 s deposition step. B) Three deposition rounds of 5 s each. After each deposition step the particles were protected by ME SAMs. C) The same as (B) but DT SAMs are used for protection. D) As (B), but without SAM protection.

From these results it can be concluded that both the DT and ME SAMs give good protection of the gold nanoparticles and prevent secondary nucleation during subsequent deposition rounds, with DT SAMs being slightly more protecting than ME SAMs. This result is not surprising, as it is known that thiols with longer *n*-alkane chains form dense layers on gold surfaces.[37] The high number of particles (187 μm^{-2}) created in the first deposition step is not repeated in subsequent deposition steps, despite protection with ME or DT. This finding indicates major consumption of active nucleation sites on the GC surface during the first deposition step. These nucleation sites are then not available in subsequent deposition experiments, and the number of particles formed in the first round cannot be reached in the following deposition rounds, despite protection of the gold particles. However, the protection mechanism to increase the number density of nanoparticles by sequential deposition is successful, as a comparison with a three-step deposition without protection, where the number density n is 41 μm^{-2}, reveals a substantially lower value of n than with protection of the nanoparticles. Coalescences of particles might be responsible for the low n value, which is also manifested by the increased particle size, as revealed by comparing the SEM images in Figure 2.

Although a DT monolayer offers slightly better insulation of the Au particles than ME, a SAM of DT has the disadvantage of being impossible to remove completely from the particles by reductive desorption within a negative potential limit at which the carbon surface or the particles themselves are not damaged, whereas ME can be reductively removed by repeatedly cycling the potential between −0.2 and −1.2 V. The possibility of removing the protective layer is important for potential analytical application of the nanoparticle-modified surface, where reductive desorption can be exploited for creating mixed monolayers.

Gold Surface Area Estimation by Oxide Layer Stripping

To understand if the achieved signal enhancement is simply due to an increase in surface area or to the properties of the deposited nanoparticles, a reliable method for estimation of the area is needed, and the electrochemical reduction of Au surface oxides to estimate the area of exposed gold[32] is used. Following the deposition of Au nanocrystals, the surface is oxidized by a potential step to 1.5 V for 5 s. Although both the Au and GC surfaces are likely to be oxidized during this applied positive potential, the oxide film on Au is selectively reduced during the reduction scan.[23,32]

A direct estimation of the gold surface area after each deposition/DT assembling process is not possible, because the DT used to protect the already-created Au nanocrystals substan-

tially suppresses the formation of an oxide layer on gold. By comparing the surface area calculated from the oxide layer reduction before and after assembling of a DT layer on nanocrystals, a 50% decrease is detected, in agreement with the trend observed by Finot et al.,[24] who reported 15 and 70% for hexanethiol and dodecanethiol, respectively. Attempts to remove DT from the nanocrystals by reductive desorption either by repeatedly cycling the potential to −1.4 V or applying a potential of −1.4 V for 10 s was not successful, since it was not possible to recover the full surface area estimated from the oxide reduction before DT assembling, which may be attributed to two sources. First, it is well established that the longer the alkyl chain length of the thiol, the more negative the peak potential required for reductive desorption, which reflects the stronger hydrophobic intermolecular interaction of the alkyl chains,[38,39] and therefore the reductive desorption attempts might have led to only partial removal of DT. Alternatively, the source of error could be damaging of the gold particles on the GC surface, due to the high applied potential.

To overcome this problem a SAM that blocks growth of already-formed gold nanoparticles during the sequential deposition procedure but does not prevent gold oxide formation could be used. Figures 2B and C reveal that the insulating effect of a ME SAM to suppress further growth of previous generations of particles during electrochemically induced nucleation is comparable to the protection by a DT SAM. In addition, the area of the oxide reduction peak of bare gold particles and of the same gold particles modified with ME differs by less than 2%, which indicates a very minor degree of blocking of the formation of an oxide layer on gold; using this ME SAM, a more accurate estimate of the surface area of deposited gold nanoparticles is achieved. Therefore, a reductive desorption step to remove the ME SAM prior to the oxide formation/reduction process is not necessary, and ME is used for protection of the gold nanoparticles during sequential deposition rounds. It is also likely that ME is oxidatively removed during the oxide layer formation step at 1.5 V, as is observed in the case of mercaptopropionic acid.[40]

The stepwise procedure of gold nanoparticle deposition, protection, and area estimation involved the following steps: 1) deposition of gold nanoparticles, 2) estimation of Au surface area by oxide layer formation and reduction, 3) protection of deposited particles by formation of a ME SAM, and 4) deposition of gold nanoparticles. Steps 1–4 are repeated (cf. Scheme 1).

The amount of gold deposited during each of the deposition/protection steps is roughly constant at a value of about 0.3 to 0.4 $\mu g\,cm^{-2}$, with the exception of the gold loading in the first deposition round, which is larger due to the higher number of nucleation sites available on a "fresh" GC surface. The gold loading is calculated from the flow of charge during the potential step, with the deposition transients corrected by background subtraction (Table 1, column 3).

Table 1. Characterization of stepwise gold nanoparticle deposition at 0 V on a GC surface.

Deposition step	Deposition time [s]	Au loading [$\mu g\,cm^2$] per deposition step[a]	Au surface area [cm^2][b]	Au surface area [cm^2][c]
1	5	0.56	0.023	0.025
2	5	0.27	0.044	0.054
3	5	0.41	0.063	0.081
4	5	0.39	0.072	0.125
5	5	0.31	0.082	–
1	25	23.68	0.124	–

[a] Calculated from background-corrected current transients during electrodeposition. [b] Estimated from the charge related to the reduction peak of the surface oxide monolayer on Au (see Figure 2) using a reported value[32] of 400 $\mu C\,cm^{-2}$. [c] Estimated from the charge of a self-assembled $FcC_{11}SH$ layer, assuming a theoretical maximal coverage[43,44] of 4.5×10^{-10} $mol\,cm^{-2}$.

A complete gold layer is plated on the GC substrate using a single potential step of 0 V for 25 s and the surface appears shiny gold with a roughness factor of 1.4, which indicates a relatively smooth gold surface. Application of a single 25 s potential step results in a 23.7 $\mu g\,cm^{-2}$ gold loading on the GC substrate, with a calculated thickness of 12 nm assuming a uniform deposition on the GC surface.

Cyclic voltammograms for the reduction of gold surface oxides of three deposition/protection cycles are presented in Figure 3. The gold surface areas can be calculated by integration of the peak areas, and the results are listed in the fourth column of Table 1. The increase of surface area during each deposition/protection round is roughly constant, thus indicating a principally surface-controlled nucleation process for each deposition step.

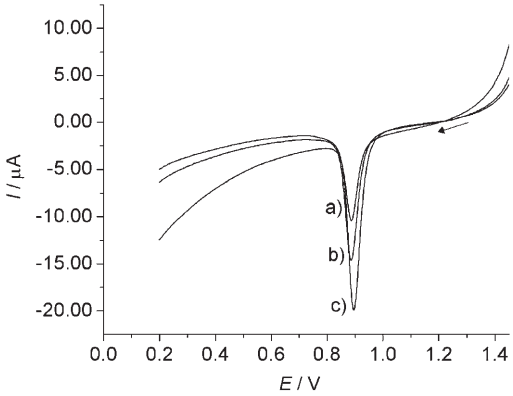

Figure 3. Voltammogram for the reduction of gold surface oxides from electrochemically deposited gold nanoparticles on GC. a) Single deposition step; b) two rounds of deposition and protection with ME; c) three rounds of deposition and protection with ME. Scan rate: 50 $mV\,s^{-1}$. The deposition potential for the gold nanoparticles was 0 V from 0.1 mM aq. $KAuCl_4$ and the length of each deposition step was 5 s.

Self-Assembling of Electroactive Monolayers

The interfacial properties of the gold nanoparticles are further investigated with a SAM of $FcC_{11}SH$, a ferrocene-terminated alkanethiol, backfilled with DT. The electroactive $FcC_{11}SH$/DT monolayer not only protects the gold nanoparticles during the sequential deposition/assembling procedure, but also allows monitoring of thiol immobilization after each deposition/protection step by measuring the diffusionless current of the covalently bound ferrocene moiety. Cyclic voltammograms for five deposition/assembling rounds from 0.1 mM $KAuCl_4$ solution, each recorded after formation of the $FcC_{11}SH$/DT SAM on the freshly deposited gold nanoparticles, are shown in Figure 4. As expected, the current increases with each deposition round, since additional ferrocene-labeled alkanethiol can be assembled on the newly created gold nanoparticles. Repeated rounds of deposition ultimately result in the saturation of nucleation centers. Consequently, additional steps of gold deposition do not lead to new nucleation centers, but instead the already-formed gold crystals grow, finally leading to a complete gold layer on the GC substrate. In this situation, additional gold deposition steps do not affect the overall gold area. For deposition from 1 mM $KAuCl_4$ the current peak levels off after the fourth deposition/SAM formation round, while for deposition from 0.1 mM $KAuCl_4$ a slight increase is still observed after the sixth deposition/SAM formation round because of a slower growth of the particles due to the lower concentration of gold ions.

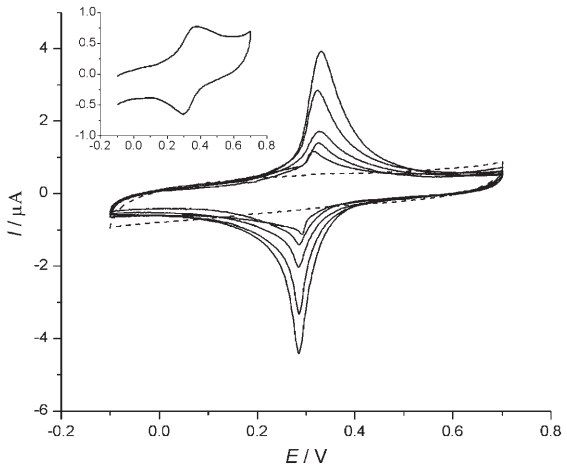

Figure 4. Cyclic voltammograms of an $FcC_{11}SH$ monolayer self-assembled on gold nanoparticles. The number of deposition rounds of the nanoparticles is one to five (with increasing peak currents). The dashed line is for a bare GC electrode and defines the background current. Inset: voltammogram of an $FcC_{11}SH$ monolayer assembled on a gold-plated GC electrode.

The performances of a GC surface completely plated with gold and of a GC surface modified with stepwise deposition of gold nanoparticles were compared in terms of formation of the $FcC_{11}SH$ electroactive SAM. The GC substrate was completely covered with gold as previously described, and the electroactive SAM prepared using the same conditions as for a five-round nanoparticle deposition, with the surface being exposed five times to solutions of $FcC_{11}SH$ and DT for backfilling to form the electroactive layer, with washing after each SAM deposition step (see Experimental Section). This procedure enables the refilling of defect sites in the monolayer with thiols and allows the bulk electrode surface and the nanoparticle surface to be directly compared.

The inset in Figure 4 shows the redox behavior of the gold-plated electrode. The charges related to the oxidation and reduction of the ferrocene end groups are $Q_A = 1.20$ and $Q_C = 1.34$ μC, respectively. The charge due to the redox reaction is increased with increasing rounds of nanoparticle deposition (see Figure 4). After five rounds the measured oxidation and reduction charges are $Q_A = 7.20$ and $Q_C = 7.26$ μC, which is a sixfold increase compared to the charge measured for a fully gold-covered GC (inset of Figure 4). The active gold area estimated by oxide layer reduction for a complete gold layer formed on the GC electrode during a single 25 s potential step to 0 V is 0.124 cm^2, while the active surface for the gold nanoparticles deposited during five 5 s potential step/SAM protection rounds is 0.082 cm^2. The increase of the redox signal and therefore of the amount of immobilized $FcC_{11}SH$ cannot be explained simply by an increase in the gold surface available for SAM formation, since the measured gold area of the nanoparticles is even slightly smaller than that of the gold-plated GC electrode. It has been established that nanometer-sized gold particles can exhibit excellent catalytic activity[41,42] due to their relatively high surface-to-volume ratio and their interface-dominated properties, which significantly differ from those of their bulk counterparts.[11,41,42] The unfavorable energetic state of surface atoms of the gold nanoparticles results in an enhanced reactivity of the metal atoms at the surface towards binding processes, in this case towards the formation of sulfur bonds, and is the likely explanation for the significant enhancement in signal, which is ninefold when normalized to the area.

The gold surface area was calculated from the charge of the self-assembled $FcC_{11}SH$ layer, assuming a theoretical maximum coverage[43,44] of 4.5×10^{-10} mol cm^{-2}, with the charge being estimated by integration of the anodic peak with correction for the charging current contribution. The theoretical maximum coverage is based on the assumption of hexagonal packing of the ferrocene moiety, with a sphere of diameter 6.6 Å.[44] The theoretical maximum coverage is in good agreement with an experimental value of 4.6×10^{-10} mol cm^{-2}, estimated by cyclic voltammetry (CV) for $FcC_{12}SH$ by Lee et al.,[43] although a value for the surface coverage of 5.9×10^{-10} mol cm^{-2} for (hydroxymethyl)ferrocene on polycrystalline gold has been reported.[45]

The gold surface areas estimated from the $FcC_{11}SH$ charge and from oxide layer formation for the first deposition round are in good agreement. However, with increasing number of deposition rounds, the difference between the areas estimated by the two methods increases, with the surface area estimated by oxide formation being smaller.

Both methods of surface area estimation have their own limitations. Gold surface area measurements by gold oxide layer formation and reduction is a simple and frequently used technique, although oxygen adsorption measurement appears to be a somewhat arbitrary procedure to determine the real sur-

face area,[46] due to the assumption of complete monolayer formation with a gold/oxygen ratio of 1:1 and to the uncertainty of the exact value of the corresponding charge required for the reduction of this monolayer, which depends on the composition of the exposed crystalline planes. However, gold surface estimation by oxide monolayer formation is widely used.[32,47] The oxide coverage on a gold-plated GC electrode as a function of potential is evaluated and is in agreement with published data.[48] For a complete gold layer, a roughness factor of 1.8 is estimated by surface oxide reduction, which is in agreement with the value reported for polished polycrystalline gold electrodes.[49] However, in the case of the deposited gold nanoparticles, the surface compromises a large part of the GC and the high anodic potential necessary for oxide layer formation on gold might introduce oxidation processes at the GC surface.[50] The interference of both oxidation processes leads to an underestimation of the surface of the gold nanoparticles arranged on the GC electrode.

Estimation of the surface area from the charge of the redox-active SAM, on the other hand, has the disadvantage that an assumption regarding the surface coverage with $FcC_{11}SH$ molecules has to be made. As the maximum theoretical value of surface coverage of 4.5×10^{-10} mol cm^{-2} is used, the values presented in Table 1 give lower limits of the real surface areas.

To summarize, although both of these methods for surface area determination result in an underestimation of the real surface area of electrodeposited nanoparticles, the area estimated by the charge of the electroactive $FcC_{11}SH$ SAM is likely to be closer to the real surface area of the gold nanoparticles than the area measured by gold oxide formation, since the area estimation by the former method gives bigger values. However, because of a lack of reliability in the accuracy of surface area measurements, we cannot correctly attribute what portion of the signal enhancement achieved is due to the area of the nanoparticles' surface as compared to the bulk gold electrode, or to the inherently improved catalytic efficiencies and favorability to form SAMs as a result of the enhanced reactivity of the surface atoms of the deposited nanoparticles.

Despite this, the large difference in the electrochemical signal of the electroactive SAM on bulk gold and on the gold nanoparticles (Figure 4) cannot be attributed to the surface area alone. The deposited area is 0.124 cm^2 for the bulk gold electrode and 0.082 cm^2 (estimated after five rounds of deposition by oxide layer formation) and 0.125 cm^2 (estimated from the charge of the electroactive SAM after four rounds of deposition) for the gold nanoparticles. Even the assumption of 100% underestimation of the surface area of the gold nanoparticles cannot explain the enhancement of the redox signal solely by the increase in surface area. The ferrocene signal of the bulk gold electrode is approximately the same only for the first round of nanoparticle deposition, despite the fact that the gold surface of the nanoparticles, as evidenced by the SEM images as well as the oxide estimation, is only a fraction of the bulk gold surface. It is therefore clear that the signal enhancement is principally due to the unique properties of nanoparticles, which makes the self-assembly processes of thiol-based monolayers more effective compared to bulk gold. This is clearly demonstrated when comparing the signal obtained from the chemisorbed electroactive SAM, where the signal obtained with the bulk gold surface is 90% less than that obtained with the deposited gold nanoparticle surface. Additionally, as the deposited nanoparticles are highly reactive, there is no need for the lengthy cleaning and activation procedures, such as chemical (e.g. piranha solution), electrochemical, and physical (e.g. polishing, UV–ozone) methods, routinely used to prepare gold surfaces prior to SAM formation.

Conclusions

Enhancement of electrochemical signals has been demonstrated using an approach of sequential electrodeposition and capping of gold nanoparticles. The electrodeposition of gold nanoparticles on GC has been optimized with regard to size and number density. The nucleation of the gold particles is fast and instantaneous, not progressive. This is a prerequisite for the successful application of the sequence of deposition/SAM protection rounds presented here, to impede secondary nucleation and increase the particle number density on the GC surface. SEM images show that the isolation of deposited nanoparticles by a SAM to prevent them from further growth in subsequent gold electrodeposition steps is successful.

The estimation of the surface area of the gold nanoparticles by oxygen adsorption is likely to be complicated by the interference of anodic processes at the GC surface at the negative potentials necessary for oxygen adsorption. This leads to an underestimation of the active gold area. Area estimation was also performed by self-assembling an electroactive layer ($FcC_{11}SH$) on the gold particles and measuring the charge. This method requires knowledge of the surface coverage of the electroactive molecules, and the theoretical maximum value has been assumed. Therefore, this method gives a lower limit of the active gold area. Both methods are consistent in showing an increase in surface area with subsequent deposition/protection steps.

In comparison to bulk gold, nanoparticles of gold immobilized on a GC surface show an increased affinity towards SAM formation and this can be used for signal amplification. This property is especially relevant in the context of electrochemical biosensors, where gold nanoparticles can be used as a transducer element for the anchoring of the probe biomolecule. An added advantage of the reported method is that no cleaning or activation of the gold surface, such as the use of piranha solution or UV–ozone, is required, and the alkanethiol/thiolated biomolecule can be chemisorbed immediately following the sequential rounds of deposition. The reported approach for signal enhancement that exploits highly reactive nanoparticulate surfaces will find considerable application in electrochemical biosensing, particularly DNA sensors for protein/nucleic acid detection by exploiting redox-tagged stem-loop structures,[30,31] where considerable improvement in detection limits would be expected.

Experimental Section

Materials: Potassium tetrachloroaurate(III) ($KAuCl_4$, 99.995%, Aldrich), sulfuric acid (95% v/v, Scharlau), sodium perchlorate (98%, Sigma), 2-ME (99%, Scharlau), 3-mercaptopropionic acid (99%, Acros Organics), DT (96% v/v, Aldrich), and ethanol (96% v/v, Scharlau) were used as received. 11-Ferrocenyl-1-undecanethiol ($HSC_{11}Fc$) was obtained from Prochimia (Poland). Aqueous solutions were prepared using MilliQ water (18.2 MΩ cm).

Electrochemistry: CV and potential-step experiments were carried out using an Autolab model PGSTAT 12 potentiostat/galvanostat controlled with the General Purpose Electrochemical System (GPES) software (Eco Chemie B.V., The Netherlands). A conventional three-electrode setup was used with the GC electrode as working electrode and a platinum wire counter electrode. All potentials were reported with respect to an Ag/AgCl reference electrode.

GC rods (Sigradur, HTW Hochtemperatur Werkstoffe, Germany) with a length of 7 cm and a diameter of 3 mm were pressed into two layers of heat-shrinking polyolefin tubes. One end of the rod, which served as the electrode surface, was polished using an electrode polishing pad (BAS) and further smoothed with 0.3-μm alumina slurry (Buehler) in MilliQ water. After polishing, the electrodes were carefully rinsed with water and sonicated for about 15 min. The electrodes were then washed with ethanol and water and conditioned by potential scanning from 0 to 1.2 V in 1 M $NaClO_4$ for at least five complete scans at 50 mV s^{-1}, at which the high background current due to GC oxidation diminished and a reproducible cyclic voltammogram was obtained. Afterwards, the background current of the bare electrode was measured by CV within the potential window used for probing the ferrocene redox reaction. Electrodes that showed a high background current above some arbitrarily selected reference were excluded. The electrodes were used immediately following the cleaning and conditioning steps.

Gold nanoparticles were electrodeposited on GC electrodes from a 0.5 M H_2SO_4 solution containing 0.1 mM $KAuCl_4$ by applying a potential step of 0 or 0.4 V for 5 s. For self-assembling monolayers of alkanethiols on gold nanoparticle deposits, the electrodes were maintained in a 2 mM ethanolic solution of the thiol (50 μL) for at least 2 h at room temperature (22 °C). The SAM of $HSC_{11}Fc$ was formed on freshly deposited gold nanoparticles by covering the electrode surface with 2 mM $HSC_{11}Fc$ (50 μL) in ethanol. The electrodes were subsequently carefully and thoroughly washed with ethanol and later with water, followed by air drying. Before gold nanoparticle deposition, SAMs of $HSC_{11}Fc$ were placed in contact for 1 h with 2 mM ethanolic solutions of ME or DT for backfilling. Following this backfilling step, a slight decrease of the ferrocene peaks was observed due to reorganization of ferrocene-terminated alkanethiols. To exclude the possibility of immobilization/adsorption of $HSC_{11}Fc$ on GC, a bare GC electrode was immersed overnight in a 2 mM $FcC_{11}SH$ ethanolic solution. The voltammogram with this electrode did not show any peaks related to the redox reactions of the ferrocene terminal entities.

The amount of gold deposited on GC (gold loading) was estimated from the charge consumed during the deposition process, which was obtained by integrating the area under the current transient curve and subtracting the charging current for a bare electrode.

The area of the deposited gold nanoparticles was estimated from the charge consumed for reduction of a formed gold oxide monolayer. For the formation of these oxide layers on the electrodeposited Au particle surfaces, a potential step of 1.5 V was applied for 5 s. The formed oxide layer was reduced by scanning the potential from 1.5 to 0 V in 0.5 M H_2SO_4 solution with a scan rate of 50 mV s^{-1}, and the surface area was estimated from the charge consumed during reduction of the oxide monolayer of Au using a reported[32] value of 400 μC cm^{-2}.

SEM for characterization of gold nanoparticles on a GC electrode was carried out using a Fei Quanta 600 environmental scanning electron microscope at an acceleration voltage of 20 kV and a working distance of 10 mm in a high-vacuum mode. Image analysis was performed with the ImageJ software (ver. 1.37v).[33]

Acknowledgements

This paper partly describes work undertaken in the context of the EC IST project Integrated Microsystem for the Magnetic Isolation and Analysis of Single Circulating Tumor Cells for Oncology Diagnostics and Therapy Follow-up (MASCOT) FP6-2005-IST-027652. The IST program is partially funded by the European Commission. Financial support by the SAFE Network of Excellence (LSHB-CT-2004-503243) is also acknowledged.

Keywords: electrochemistry · gold · monolayers · nanoparticles · self-assembly

[1] D. Hernández-Santos, M. B. Gonzalez-Garcia, A. C. Garcia, *Electroanalysis* **2002**, *14*, 1225–1235.
[2] S. G. Penn, L. He, M. J. Natan, *Curr. Opin. Chem. Biol.* **2003**, *7*, 609–615.
[3] A. N. Shipway, E. Katz, I. Willner, *ChemPhysChem* **2000**, *1*, 18–52.
[4] E. Katz, I. Willner, J. Wang, *Electroanalysis* **2004**, *16*, 19–44.
[5] X. L. Luo, A. Morrin, A. J. Killard, M. R. Smyth, *Electroanalysis* **2006**, *18*, 319–326.
[6] C. W. Welch, R. G. Compton, *Anal. Bioanal. Chem.* **2006**, *384*, 601–619.
[7] R. Narayanan, M. A. El-Sayed, *J. Phys. Chem. B* **2005**, *109*, 12663–12676.
[8] *Nanoparticles made in Mesoporous Solids*, L. M. Bronstein in *Colloid Chemistry 1, Top. Curr. Chem., Vol. 226*, Springer, Heidelberg, **2003**, pp. 55–89.
[9] J. D. Aiken, R. G. Finke, *J. Mol. Catal. A* **1999**, *145*, 1–44.
[10] B. F. G. Johnson, *Coord. Chem. Rev.* **1999**, *190–192*, 1269–1285.
[11] M. Haruta, *Catal. Today* **1997**, *36*, 153–166.
[12] M. S. El-Deab, T. Ohsaka, *Electrochem. Commun.* **2002**, *4*, 288–292.
[13] M. S. El-Deab, T. Ohsaka, *J. Electroanal. Chem.* **2003**, *553*, 107–115.
[14] C. R. Raj, A. I. Abdelrahman, T. Ohsaka, *Electrochem. Commun.* **2005**, *7*, 888–893.
[15] C. X. Xu, J. X. Su, X. H. Xu, P. P. Liu, H. J. Zhao, F. Tian, Y. Ding, *J. Am. Chem. Soc.* **2007**, *129*, 42–43.
[16] C. R. Raj, T. Okajima, T. Ohsaka, *J. Electroanal. Chem.* **2003**, *543*, 127–133.
[17] L. Zhang, X. Jiang, *J. Electroanal. Chem.* **2005**, *583*, 292–299.
[18] M. T. Castaneda, S. Alegret, A. Merkoci, *Electroanalysis* **2007**, *19*, 743–753.
[19] M. T. Castaneda, A. Merkoci, M. Pumera, S. Alegret, *Biosens. Bioelectron.* **2007**, *22*, 1961–1967.
[20] M. Brust, C. J. Kiely, *Colloids Surf. A* **2002**, *202*, 175–186.
[21] M. S. El-Deab, T. Sotomura, T. Ohsaka, *J. Electrochem. Soc.* **2005**, *152*, C730–C737.
[22] M. S. El-Deab, T. Sotomura, T. Ohsaka, *J. Electrochem. Soc.* **2005**, *152*, C1–C6.
[23] M. O. Finot, G. D. Braybrook, M. T. McDermott, *J. Electroanal. Chem.* **1999**, *466*, 234–241.
[24] M. O. Finot, M. T. McDermott, *J. Electroanal. Chem.* **2000**, *488*, 125–132.
[25] F. F. Gao, M. S. El-Deab, T. Okajima, T. Ohsaka, *J. Electrochem. Soc.* **2005**, *152*, A1226–A1232.
[26] L. Zhang, X. U. Jiang, E. K. Wang, S. J. Dong, *Biosens. Bioelectron.* **2005**, *21*, 337–345.
[27] M. S. El-Deab, T. Okajima, T. Ohsaka, *J. Electrochem. Soc.* **2006**, *153*, E201–E206.
[28] C. E. D. Chidsey, C. R. Bertozzi, T. M. Putvinski, A. M. Mujsce, *J. Am. Chem. Soc.* **1990**, *112*, 4301–4306.
[29] H. X. Ju, D. Leech, *Phys. Chem. Chem. Phys.* **1999**, *1*, 1549–1554.

[30] C. H. Fan, K. W. Plaxco, A. J. Heeger, *Proc. Natl. Acad. Sci. USA* **2003**, *100*, 9134–9137.
[31] A. E. Radi, J. L. A. Sanchez, E. Baldrich, C. K. O'Sullivan, *J. Am. Chem. Soc.* **2006**, *128*, 117–124.
[32] S. Trasatti, O. A. Petrii, *Pure Appl. Chem.* **1991**, *63*, 711–734.
[33] http://rsb.info.nih.gov/ij.
[34] G. Staikov, W. J. Lorenz, E. Budevski, *Electrochemical Phase Formation and Growth*, Wiley-VCH, Weinheim, **1996**.
[35] J. Strutwolf, M. Wunsche, H. Meyer, R. Schumacher, *Z. Phys. Chem.* **1999**, *208*, 239–251.
[36] H. Yang, T. H. Lu, K. H. Xue, S. G. Sun, S. P. Chen, *J. Appl. Electrochem.* **1997**, *27*, 428–433.
[37] H. O. Finklea, S. Avery, M. Lynch, T. Furtsch, *Langmuir* **1987**, *3*, 409–413.
[38] T. Kondo, T. Sumi, K. Uosaki, *J. Electroanal. Chem.* **2002**, *538*, 59–63.
[39] C. J. Zhong, M. D. Porter, *J. Electroanal. Chem.* **1997**, *425*, 147–153.
[40] C. A. Canaria, J. So, J. R. Maloney, C. J. Yu, J. O. Smith, M. L. Roukes, S. E. Fraser, R. Lansford, *Lab Chip* **2006**, *6*, 289–295.
[41] A. N. Shipway, M. Lahav, I. Willner, *Adv. Mater.* **2000**, *12*, 993–998.
[42] M. Králik, A. Biffis, *J. Mol. Catal. A* **2001**, *177*, 113–138.
[43] L. Y. S. Lee, T. C. Sutherland, S. Rucareanu, R. B. Lennox, *Langmuir* **2006**, *22*, 4438–4444.
[44] P. Seller, J. D. Dunitz, *Acta Crystallogr. Sect. B* **1979**, *35*, 2020–2032.
[45] S. E. Creager, L. A. Hockett, G. K. Rowe, *Langmuir* **1992**, *8*, 854–861.
[46] J. C. Hoogvliet, M. Dijksma, B. Kamp, W. P. van Bennekom, *Anal. Chem.* **2000**, *72*, 2016–2021.
[47] J. S. Gordon, D. C. Johnson, *J. Electroanal. Chem.* **1994**, *365*, 267–274.
[48] B. Piela, P. K. Wrona, *J. Electroanal. Chem.* **1995**, *388*, 69–79.
[49] R. T. Carvalhal, R. S. Freire, L. T. Kubota, *Electroanalysis* **2005**, *17*, 1251–1259.
[50] X. G. Zhang, Y. Murakami, K. Yahikozawa, Y. Takasu, *Electrochim. Acta* **1997**, *42*, 223–227.

Received: November 27, 2007
Published online on March 25, 2008

